CONF-970126--Draft
LA-UR--96-4506 DRAFT

APPLICATIONS OF A VERSATILE NEW INSTRUMENT MODULE

G. S. Brunson and G. J. Arnone
Los Alamos National Laboratory, Los Alamos, NM 87545

We have found a number of interesting applications for the Pulse Arrival Time Recording Module (PATRM). This CAMAC module is capable of recording the arrival time of up to 4 million pulses. The result is a list of 32-bit binary numbers in which each number represents the arrival time of a single pulse expressed in terms of the number of "ticks" of a 10MH clock which have elapsed since the beginning of the count. The versatility arises from the fact that the data list can be analyzed by whatever algorithm we can put into software, and that we can "play it back" as many times as we like. We already have the following applications:

1. Neutron multiplicity counting in waste assay.
2. Study of dead-time recovery and double pulsing in individual channels.
3. Auto-correlation analysis for Rossi-α measurements in critical systems.
4. Variable channel width multichannel scaler for delayed neutron counting.
5. Cross-correlation analysis and conventional multi-scaling.
6. Time dependent multiplicity measurements during neutron interrogation.

We expect in the coming year to test an updated version of the PATRM which will incorporate a 100MH clock and label each pulse with the channel from which it came. The device will be configured as a single PC card installable in any high performance IBM type computer.

INTRODUCTION

The Pulse Arrival Time Recording Module (PATRM) is extremely simple in principle. It records the arrival time of each pulse up to total of 4 million. The result is a list of 32-bit binary numbers each of which records the arrival time of a particular pulse (in 10 MH "ticks" since the beginning of the count). The "Swiss army knife" versatility arises from the fact that the list file records all that we can ever know about that particular segment of the data stream; we can analyze that data with any algorithm for which we can write the software. Moreover, we can "play it back" and try different algorithms on exactly the same data. Physically, the PATRM is a double-wide CAMAC module with 15 independent pulse inputs. See Fig. 1. If several pulses happen to arrive on the same tick of the clock, none is lost. They will be recorded in sequential locations in the list with their arrival times differing by just one tick. The electronic details of the PATRM have been described elsewhere.[1] All experiments described in this paper (except Rossi-α) were carried out with highly moderated 4-π neutron counters of high sensitivity (>15%). The Rossi-α measurements were in a critical system in which it is not practical to state a sensitivity. In all cases, the signal sources were ^{3}He-filled proportional counter tubes.

This paper deals primarily with 'passive' measurement, meaning that there is no interrogating burst of neutrons. 'Active' measurement with interrogation by bursts of neutrons has been discussed elsewhere and is the subject of a paper by Hollis and Melton in these proceedings. There was also an earlier paper by Hollis, et al.[2]

PHANTOM SHIFT REGISTER

The original rationale for this device came from Ken Coop, who anticipated that it would be a significant improvement on the shift register which we had been using for neutron coincidence counting of trans-uranic waste. Earlier methods of multiplicity analysis counted neutron events in a gated scaler or the number of pulses remaining in a shift register just after a pulse has exited. Both of these methods require that the analysis parameters (window width, clock rate, etc.) be set before collecting data. To try different parameters required rerunning the entire experiment. Using the PATRM to record the raw data list, we can "play it back" with different parameters or even a completely different algorithm for comparative analysis.

The term "phantom shift register" refers to a software analog to the usual hardware shift register. Starting with the first pulse arrival time (t1), we add the window width (say, 100 μsec = 1000 ticks of the 10MH clock) to that time to get the far boundary of the first window. We scan the list between t1 and (t1+1000) to count the number of pulses in that interval. We find n pulses in the window (n can be 0) and we increment by one the nth bin in our triggered window histogram. We move on to the second pulse at t2 (which may, or may not, have fallen in the preceding window) and inspect the list for events between t2 and (t2+1000), again tallying the result in the histogram. And so on to the end of the list. When through, we have a histogram which represents the number of times that exactly n pulses (n=0,1,2...) have been observed in a triggered window. This is normalized to unity so that each bar in the histogram represents the probability that exactly n pulses will be observed in a given window.

Next we do another scan of the entire list using arbitrarily placed windows of the same 1000 tick width.

We scan the list for pulses between t=0 and t=1000, between t=1000 and t=2000, and so on. Each time we tally the result in a separate histogram which represents the number of times that exactly n pulses (n=0,1,2...) have been observed in an arbitrary window. This is also normalized to give the probability for n pulses in such a window. Figure 2 illustrates the two histograms obtained by counting a 10-gram sample of plutonium metal in a counter of ~32% sensitivity with a 100 μsec window. Note the logarithmic vertical scale. Higher multiplicities occur rarely; and triggered windows are much more apt to see higher multiplicities.

These two probability histograms are the input to the multiplicity analysis algorithm, whether it be the Hage[3] technique or the one used in this group.[4] These algorithms are not discussed here since they have been covered in the cited documents. A major advantage of the PATRM is that while assembling the above histograms, we can exclude from analysis any single window which has too many pulses in it and therefore might be attributable to a cosmic ray event. The multiplicity level at which we exclude is set by the operator. For a relatively low sensitivity counter, we might set n=5. For a more sensitive counter, or for multiplying samples, it might be n=10 or more. If we are uncertain, we can play it back with a different criterion. Typically, this requires about one minute.

Another feature of the software permits us to "capture", and set aside for later analysis, a segment of the data stream with a very large number of pulses. In a large counter such as CTEN,[5] we occasionally observe a cosmic ray shower which can register as many as 50 or more events in a window. The threshold of interest is set by the operator. Figure 3 illustrates such an event. The Fig. 3a depicts the pulses as distributed in a 500 μsec window. The Fig. 3b shows the same events binned in a histogram. This feature is helpful in diagnosing electronic noise, since, in general, noise will not exhibit the die-away characteristic of neutrons in the counter.

At our elevation (~6750 feet), we see large cosmic ray events in CTEN from a few times a night to a few times per hour, depending on the criterion for capture. In Fig. 3a, we see a few pulses at the leading edge of the window, a small gap, and then the decay of neutron pulses in a manner commensurate with the time characteristics of the detector. We see this consistently with large events and we think such a data pattern is triggered by mesons. The interval between the triggering events

and the rest of the pulses can vary considerably. Figure 4 illustrates an unusual case in which the interval is ~ 15 μsec.

AUTO-CORRELATION

While executing the shift-register algorithm described above, we can also do auto-correlation on the same data. As we examine each window (in the first pass), we not only count the number of pulses in the window, we also sort them, one by one, into 100 bins[a] depending on where each one fell in the window. This generates an auto-correlation distribution spanning whatever time the operator specified for the window width. Figure 5 is an example of such a distribution derived from the same data list as Fig. 2. Auto-correlation makes a number of useful things possible.

Examination of Dead-time Recovery in Counting Channels

This section is more detailed than the others for two reasons: Dead time recovery and double pulsing are vital factors in multiplicity counting; and the other applications mentioned in this paper have been, or will be, described elsewhere.

Figure 6 illustrates the auto-correlation observed in a single channel when counting a large AmLi (α,n) source. The source was random, and except for dead-time effects, should show no correlation. This data was obtained while we were comparing a new pulse channel design with a conventional channel which we have been using for a number of years. The new unit (PADM)[6] incorporates four independent channels (Preamplifier, Amplifier, and Discriminator) in a single Module. The time constant in each channel can be set at 0.5, 1, 2, or 4 μsec. In Figure 6, the five curves represent respectively from the left the response of the PADM at 0.5 μsec, PADM at 1 μsec, the conventional channel at nominally 1 μsec, PADM at 2 μsec, and PADM at 4 μsec. For the several ^{3}He counters that we have examined in this way, we find that the dead time recovery can best be modeled by a linear term. Figure 6 differs from Fig. 5 in two distinct ways:

1. Figure 6 is uncorrelated; Figure 5 shows a strong correlation.

---

[a] This is set by the software and could be any reasonable number. For our purposes 100 is convenient.

2. In Fig. 6, the count goes to 0 at 0 time. In Fig. 5, the count is depressed by only ~20% because the data represents the output of five roughly equal channels only one of which is affected by the dead time of the pulse which triggered the window.

All five of the curves in Fig. 6 show a hump just at the end of dead-time recovery. We conjecture that this represents interactions between two neighboring pulses in which the tail of the first pulse boosts over the discriminator threshold a small pulse which would not otherwise have "made the grade." This attribution is supported by the fact that the probability of an extraneous pulse is (within statistics) proportional to the count rate, that is proportional to the proximity of pulses to each other.

Figure 7a shows the auto-correlation curves for a module consisting of three 2" x 40" 4 atm ^{3}He detectors in parallel. The three curves correspond respectively to the three discriminator levels indicated on the pulse height spectrum in Fig. 7b. The detectors and cabling in this module have a combined capacitance of ~ 80 pf. Normally we connect these modules in groups of three (9 detectors in all). When we connected 3 modules to the same channel (~ 275 pf including a few additional feet of cable), there was no perceptible effect due to the additional capacitive load. In any event, the anomalous counts represent a small effect. as seen in the following table which refers to the data in Fig. 7:

Curve	Discriminator	Count Rate	Anomalous Fraction
1	0.400	2760	0.13%
2	0.600	2720	0.09%
3	0.800	2700	0.04%

We emphasize here that the different count rates in the above table refer to different discriminator settings at the same neutron intensity, whereas the proportionality to count rate mentioned in the preceding paragraph applies to different neutron intensities at the same discriminator setting.

In contrast to the ^{3}He detectors discussed above, Fig. 8a illustrates double pulsing in a 2" x 20" 15 atm ^{4}He detector. All curves are normalized to 10^6 events. The upper curve shows data taken at ~ 1430 counts/sec. The second curve was made at ~ 440 counts/sec (same discriminator setting, reduced neutron intensity). The fact that the anomalous counts are essentially the same for the two

instances indicates that they arise from double pulsing (interaction of pulse with discrimnator rather than with another pulse). The other two curves illustrate the effect of raising the discriminator level. The following table shows the trade-off between sensitivity and double-pulsing.

Curve	Discriminator	Counts/sec	% Double Pulsing
1	0.200	1430	11.3
3	0.300	680	3.3
4	0.400	420	0.67

Curve 2 is not tabulated because it was made at reduced neutron intensity. However, it showed 11.8% double pulsing, comparable, as it should be, to Curve 1.

For completeness, we include in Fig. 9a the auto-correlation data for a Westinghouse fission chamber loaded with about half a gram of ^{235}U. The discriminator was set as shown on the pulse height spectrum in Fig. 9b. This data was taken at 1000 volts, but there was no perceptible difference in the recovery characteristic when the voltage was reduced to 50.

Dead-time Correction in Multiplicity Counting

In multiplicity counting, dead-time losses are much more severe than they are in counting in the general case. We take the auto-correlation distribution and use the Levenberg-Marquardt algorithm to fit a single exponential function plus a background. This is modified by a linear dead-time recovery term spanning (for this detector) 10μsec. Figure 10 shows such a fit on the data of Fig. 5. To repeat in other words what was said above, the nth data point in the figure represents the number of times that a pulse was found n μsec behind another pulse. The triangular area between the two smooth curves represents the actual number of pulses lost in dead-time. These losses amounted to 726 counts. The total count was 112,005 in 500 sec, for a count rate of 224 s^{-1}. Thus the actual losses were:

726/112,005 = 0.65%.

On the other hand, if we estimate losses based merely on count rate, the result is quite different. Assume a system dead-time of 1 μsec (a five channel system with a nominal dead time of 5 μsec per channel), we have losses of :

$$.000001 * 224 = 0.022\% ,$$

which would be low by a factor of ~ 30.

One approach we have taken on the dead-time problem is to "put back" the lost pulses. We have written a Monte Carlo routine with which we scan the data list and insert in a random but realistic way the lost pulses. Figure 11 is the auto-correlation curve obtained when we process the "dead-time corrected" list. From this, we generate another pair of histograms (slightly different from Fig. 2) which serve as input to the multiplicity algorithms mentioned above.

Rossi-α

Rossi-α is a measurement routinely made on many critical or near critical nuclear systems.[8,9,10,11] In its simplest form, we do an auto-correlation on the pulse train coming from neutron detectors located (preferably) deep within the assembly. From the auto-correlation distribution, we obtain an exponential curve which characterizes the average time behavior of neutron chains in that system. This enables us to infer a prompt neutron life-time as well as examine other aspects of the system near critical.

Rossi-α measurements are currently being made on SHEBA[b] at this installation. The neutron pulses are obtained from four small high-pressure ^{3}He detectors located in a well near the center of

---

[b] SHEBA is a uranyl fluoride solution system. The solution contains ~1 g/cc of uranium (~5% enriched). The cylindrical tank with vertical axis has an ID of 19.25 in. Delayed critical is reached when the tank is filled to a depth of ~20 in.

the tank. To reduce dead-time losses, we lead the signals independently to four separate channels of a PADM module described above.

Figure 12 displays a Rossi-α distribution observed in SHEBA by Rene Sanchez using the list module (PATRM). The system was about \$3 below delayed critical. The coincidence distribution has been fitted with two exponential terms plus a background continuum. These components are plotted individually in the graph. The longer exponential represents the fundamental characteristic of the system, while the short one is due to higher mode(s). For data taken nearer delayed critical, the shorter exponential becomes almost invisible.

SHEBA, having only one region, is a simple system. In other systems having reflectors and possibly more than one multiplying region, Rossi-α measurements can yield information regarding time characteristics of the various regions and neutron communication between regions. For this purpose, we do the measurements by cross-correlation between detectors located in different regions.

The improved PATRM now being designed will make this very easy, because every pulse will be tagged with the channel of origin. With this additional information, any conceivable cross-correlation can be written into the software. We have, however, been able to do limited cross-correlation with the current PATRM even though the pulses, per se, are not tagged.

As mentioned above, if multiple pulses arrive on the same tick, they will be recorded as having arrived on successive ticks. We choose a specific counter channel to serve as the "trigger" channel to be cross-correlated with all the other channels. We "fan out" the pulse from the trigger channel into three separate inputs to the PATRM. Figure 13 shows a short segment of a data list made in this way. The triplets in the list (indicating the occurrence of a trigger) are bracketed. In scanning the list, the software opens a window only when it encounters a triplet; it ignores triplets within any window. Of course, there is the possibility of a triplet really occurring during a count. This can only occur in the unlikely event of three independent pulses arriving within the span of 0.3 μsec. With plausible count rates the chance of this happening is on the order of 10^{-6}.

MULTI-CHANNEL SCALING

The PATRM can be used as a conventional multi-channel scaler if the cross-correlation software is modified slightly. We merely ignore any triggers until after a window has been closed and start another window with the next following trigger. We have complete control, in software, of the number and width of the time channels. A feature of the PATRM not now used is the capability of scaling the clock frequency down by 2^n where n can range up to 7. In principal, time channels can be set from 10^{-7} sec to several minutes and the number of channels from a few to thousands. The only restriction is capacity of the memory: 4 million events.

With a somewhat different application of multi-scaling, David Loaiza is currently doing measurements of delayed neutrons at this installation. To this end, we have written special software to use the PATRM as a single-pass multi-scaler with variable width time bins.. The execution of the experiment entails three steps:

1. Neutron irradiation of a small sample of fissionable material with the GODIVA critical assembly. The sample may be exposed over a period of time long enough to saturate the population of delayed neutron precursors, or it may be exposed to a burst irradiation Both are used.
2. The sample is transported pneumatically to a well shielded neutron counter. Transport time is ~150 msec.
3. Counting follows for ~ 5 minutes, during which time the count rate diminishes from 5 x 10^4 s^{-1}, or higher, to a background (<10 s^{-1}).

The software for taking data under these conditions does the folowing:

1. Starts the clock in the PATRM when a sensor detects the departure of the sample from the irradiation position. This means that the time reference in the list is tied to a well-defined and reproducible event.
2. Does not enable neutron inputs to the PATRM until another sensor detects the arrival of the sample at the counting station. This avoids recording neutrons not associated with the sample.
3. Scans the data list with windows (bins) of increasing width to acommodate the four orders of magnitude change in count rate during the decay of the sample. Currently, we start with time bins 20 msec wide and double the width every 50 bins.

Figure 14 shows the the data (used by permission) resulting from such a counting routine. Figure 14a plots the entire run; the ordinate (log scale) is the count rate; the abscissa is time in seconds since the irradiation. Time is reckoned to the midpoint of each bin. The four smaller figures (linear ordinate scale) present the same data piece-wise for a more detailed view.

NEUTRON BURST INTERROGATION AND AUTO-CORRELATION

Charles Hollas has developed software to utilize the PATRM in correlation measurements of TRU waste when it is interrogated by bursts of neutrons from a small D-T neutron generator. He is discussing this in a separate paper in this meeting.

CONCLUSION

We want, by the foregoing examples, to emphasize the versatility of the present PATRM and the even greater potential of the new design. The improved version will record all that can ever be known from a given signal stream. Whatever data treatment is desired can be written into the software, and alternative analyses can be applied to exactly the same data.

Captions

Fig. 1. Pulse Arrival Time Recording Module (PATRM)

Fig. 2. Probability histogram obtained with the "phantom shift register." The sample was 10-gr of plutonium metal (~ 5% ^{240}Pu). In each pair of bars, the one on the left represents the probability that exactly n pulses will be counted in an arbitrary 100-μsec window. The bar on the right corresponds to the probability that n pulses will be found in a 100-μsec window triggered by a neutron pulse. Logarithmic vertical scale.

Fig. 3. Cosmic ray shower in the CTEN counter. Upper figure shows the distribution of events in a 500-μsec segment of the data list. There is a small gap between the meson events that triggered the window and the following neutrons. In the lower figure, the events are sorted into 25 μsec time bins, showing the characteristic decay of a neutron burst.

Fig. 4. Cosmic ray shower with unusually long interval (15 μ sec) between mesons and neutrons.

Fig. 5. Auto-correlation distribution of neutron pulses. This is from the same data list as the probability histogram in Fig. 2.

Fig. 6. Auto-correlation of pulses from an uncorrelated souirce (AmLi) using different preamplifier time constants. The traces are (1) PADM @ 0.5 μsec time constant, (2) PADM @ 1.0 μsec, (3)conventional counter channel at nominal 1 μsec, (4) PADM @ 2 μsec, and (5) PADM @ 4 μsec.

Fig. 7. Auto-correlation distribution obtained in counting an uncorrelated source (AmLi) with a pod of three 2" x 40" ^{3}He detectors at three different discriminator settings. The respective settings are displayed on a plot of the pulse height spectrum in the lower figure.

Fig. 8. Auto-correlation distribution obtained in counting an uncorrelated source (AmLi) with a ^{4}He

(2" x 20", 15 atm) at three different discriminator settings. The top two curves were made at the same setting, but with the neutron intensity decreased by moving the source away. See the table. The discriminator levels are shown on the pulse height spectrum in the lower graph.

Fig. 9. Auto-correlation distribution obtained in counting an uncorrelated source (AmLi) with a fission chamber loaded with about 1/2 g ^{235}U. Discriminator level shown in lower graph.

Fig. 10. Auto-correlation distribution (same as in Fig. 5) fitted with a single exponential plus background. this is modified with a linear dead time recovery term for the first 10 μsec. The smooth curve represents the distribution inferred for an ideal counter with no dead time.

Fig. 11. Auto-correlation distribution of the data in Fig. 10 after the dead-time losses have been "put back" with a Monte Carlo routine.

Fig. 12. Auto-correlation in SHEBA to measure Rossi-α Logarithmic vertical scale. The three straight lines represent the components of the fitting model:

Fig. 13. Short segment of a data list illustrating the "triplets" which mark trigger pulses.

Fig. 14. Using the PATRM as a single-pass multi-channel scaler with variable width time bins to record the delayed neutron die-away. Top graph (log vertical scale) shows a complete run. The other four curves display (with linear vertical scale) segments of the whole. We begin with 20 msec bins and double the bin width after every 50 bins, using 5.12 sec bins toward the end of a 5 min count.

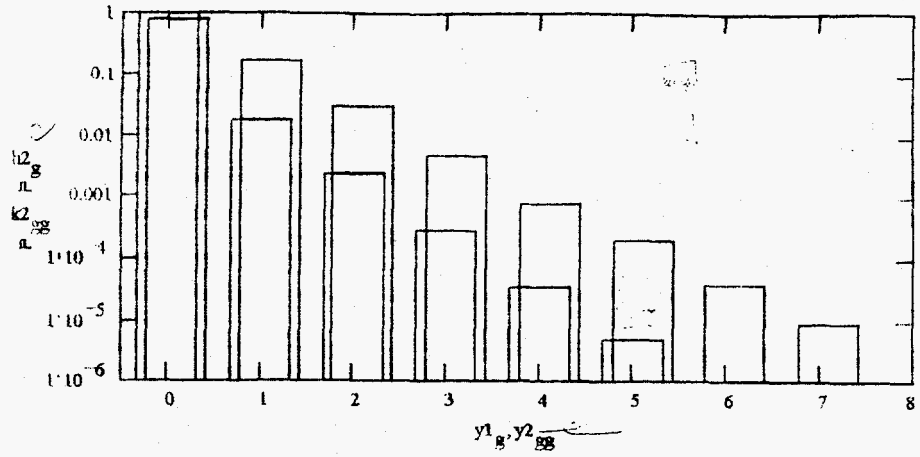

Path: J:\WINMCAD\SLDOC
File: SLFIG2 .PRN

0.9805	0.7978
0.01701	0.1681
0.0022	0.02842
0.000276	0.004566
3.4e-005	0.000798
4e-006	0.000179
1e-006	3.2e-005
0	1e-005
0	9e-006

DISCLAIMER

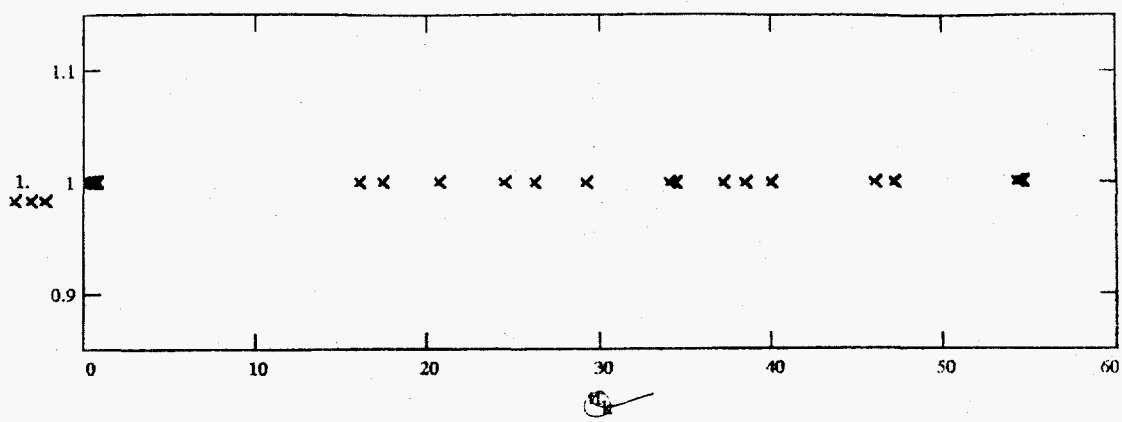

Path: J:\WINMCAD\SLDOC
File: SLFIG4 .PRN

```
   0
 0.2
 0.4
 0.6
 0.8
  16
17.4
20.6
24.4
26.2
29.2
  34
34.4
37.2
38.4
  40
  46
47.2
54.2
54.4
54.6
62.2
  63
69.8
75.8
  76
81.6
82.8
83.2
90.8
93.8
96.2
```

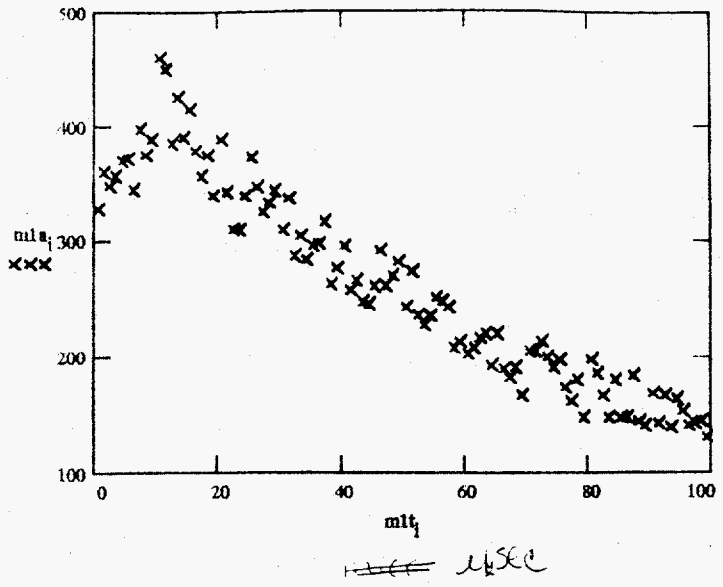

Path: J:\WINMCAD\SLDOC
File: SLFIG5 .PRN 1,800 .

0.5	327		
1.5	360		
2.5	348		
3.5	357	Path:	J:\WINM
4.5	371	File:	SLFIG5
5.5	373		
6.5	344	57.5	243
7.5	399	58.5	209
8.5	375	59.5	213
9.5	389	60.5	203
10.5	460	61.5	209
11.5	450	62.5	218
12.5	386	63.5	220
13.5	425	64.5	193
14.5	391	65.5	221
15.5	416	66.5	190
16.5	380	67.5	183
17.5	357	68.5	191
18.5	376	69.5	167
19.5	340	70.5	206
20.5	389	71.5	206
21.5	343	72.5	213
22.5	311	73.5	200
23.5	310	74.5	191
24.5	339	75.5	199
25.5	374	76.5	174
26.5	348	77.5	162
27.5	325	78.5	181
28.5	334	79.5	148

Padm1.mcd 10/18/96 9:43 AM

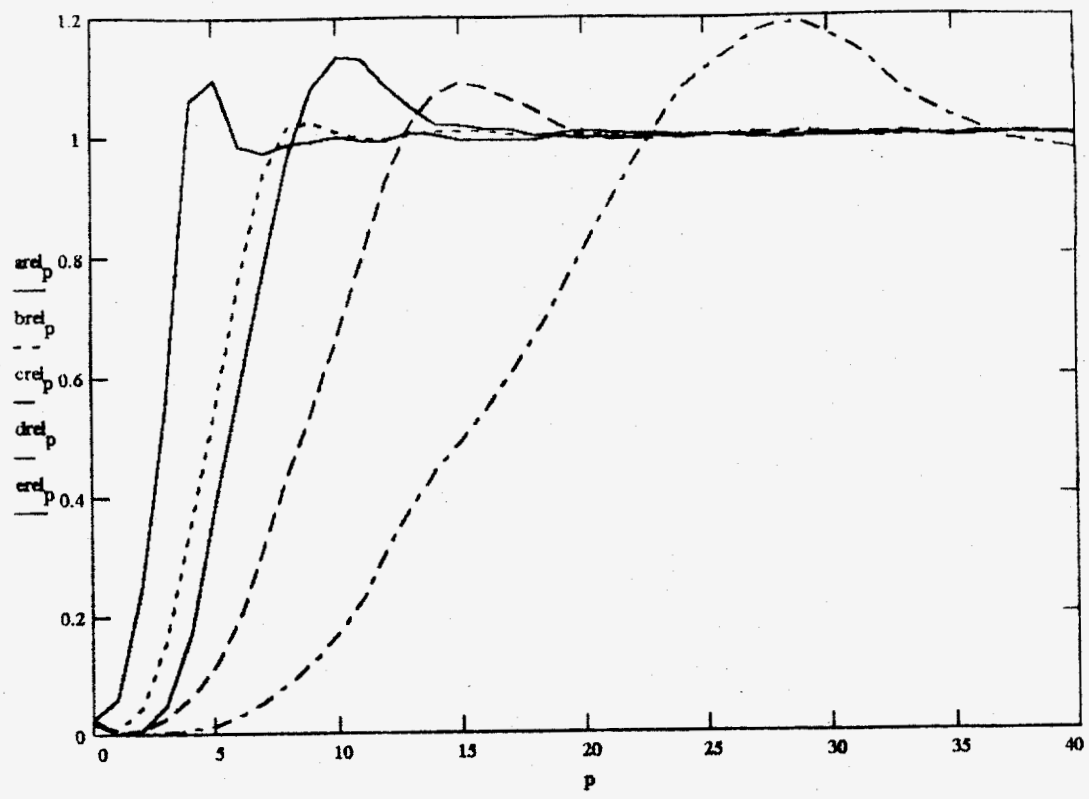

usec

Fig 6

Data in SL1166.PRN

PREAMPE 8 NOV 96 This is an effort to consolidate the results of the dead time recovery study.
These results came from the middle pod of COOP chan 2. 80 pf 1200 volts.
1 usec time constant in PADM CHAN 2. Disc @ 0.200,0.400,0.600,0.800.

$a := READPRN(kha01x) + READPRN(kha02x) + READPRN(kha03x)$ $k := 0..3600$ $i := 0..99$

$b := READPRN(khb01x) + READPRN(khb02x) + READPRN(khb03x)$

$c := READPRN(khc01x) + READPRN(khc02x) + READPRN(khc03x)$ $s_k := READ(KHAA)$ $h := 0..1900$

$d := READPRN(khd01x) + READPRN(khd02x) + READPRN(khd03x)$

$sp_h := s_{h+7}$

1, 2, 3 use same dash dist on both 7 in Acp

in file >efig 7a.prn

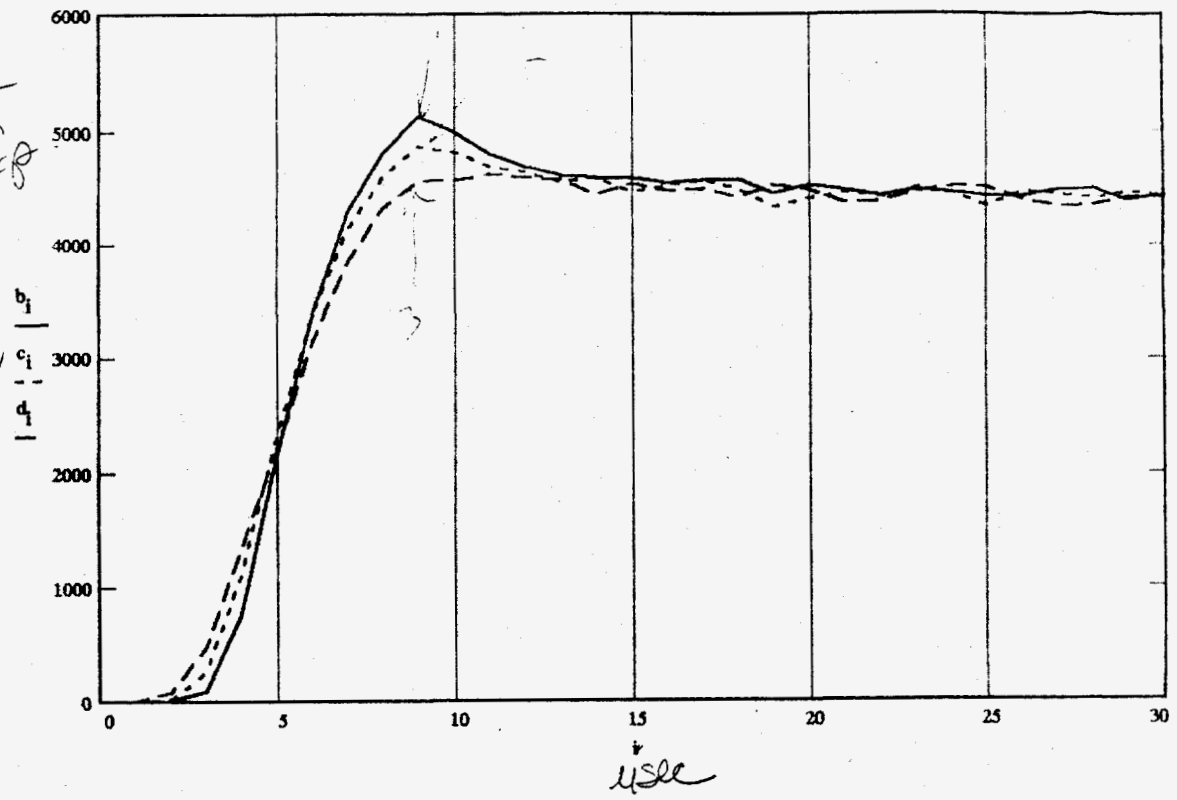

$xx1 := 60$ $xx2 := 137$ $xx3 := 214$ $xx4 := 294$

$M := 500$ $x_0 := xx1$ $y_0 := 1$ $x1_0 := xx2$ $y1_0 := 1$ $x2_0 := xx3$ $y2_0 := 1$ $x3_0 := xx4$ $y3_0 := 1$

$bb := 0..1$ $x_1 := xx1$ $y_1 := M$ $x1_1 := xx2$ $y1_1 := M$ $x2_1 := xx3$ $y2_1 := M$ $x3_1 := xx4$ $y3_1 := M$

7b in file >efig 7b.prn

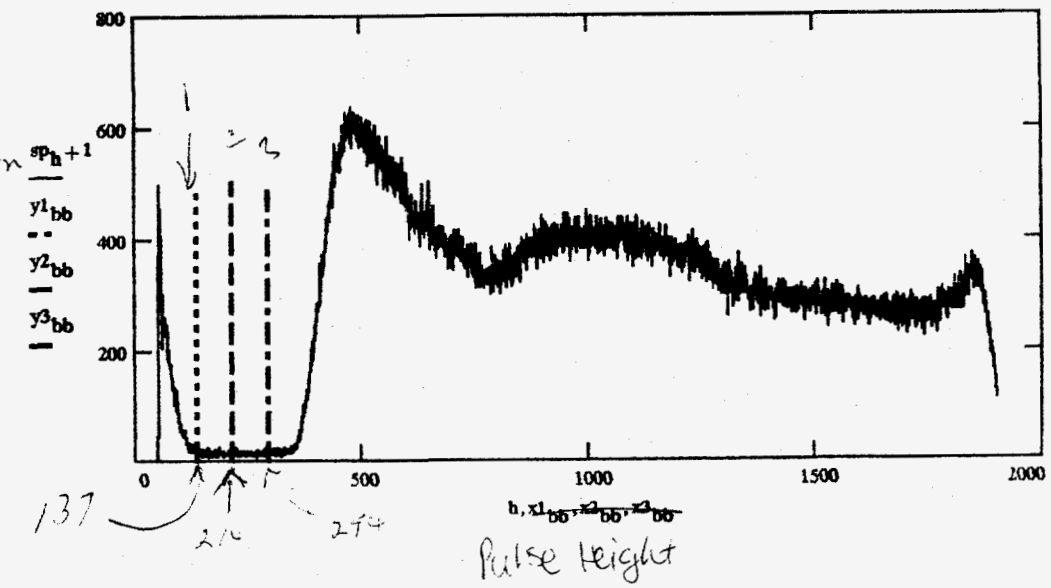

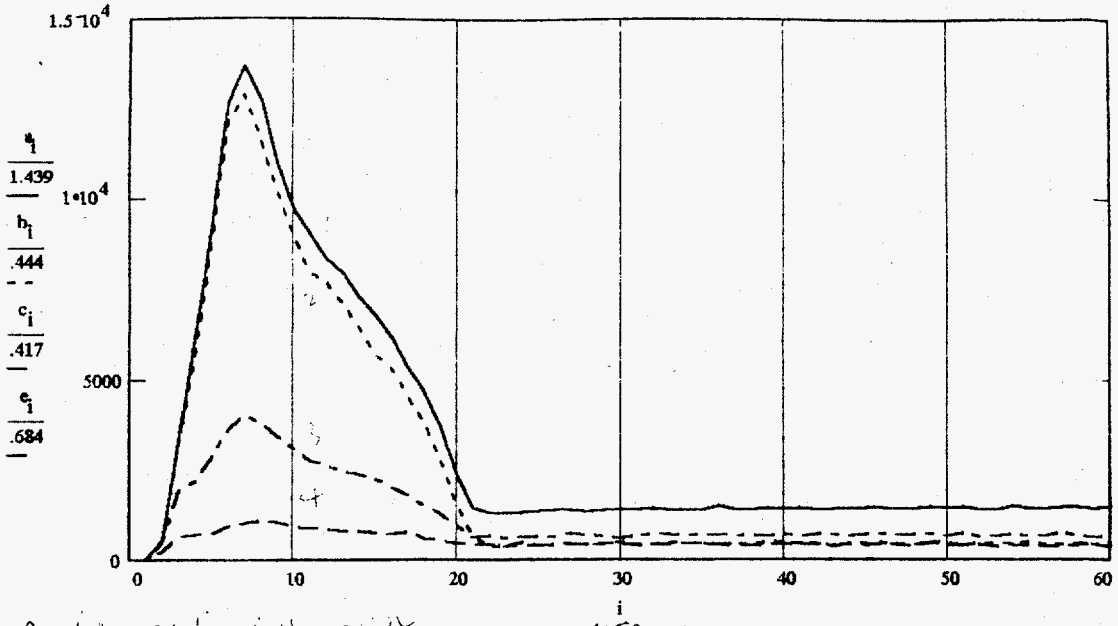

$$\sum_{v=2}^{21} (b_v - L2) = .444$$

$$\sum_{v=2}^{21} (c_v - L3) = .417$$

$$\sum_{v=2}^{21} (d_v - L4) = .226$$

$M := 9$ $x_0 := 59$ $y_0 := 1$ $x1_0 := 136$ $y1_0 := 1$ $x2_0 := 212$ $y2_0 := 1$ $x3_0 := 98$ $y3_0 := 1$

$bb := 0..1$ $x_1 := 59$ $y_1 := M$ $x1_1 := 136$ $y1_1 := M$ $x2_1 := 212$ $y2_1 := M$ $x3_1 := 98$ $y3_1 := M$ $s_k := REA$

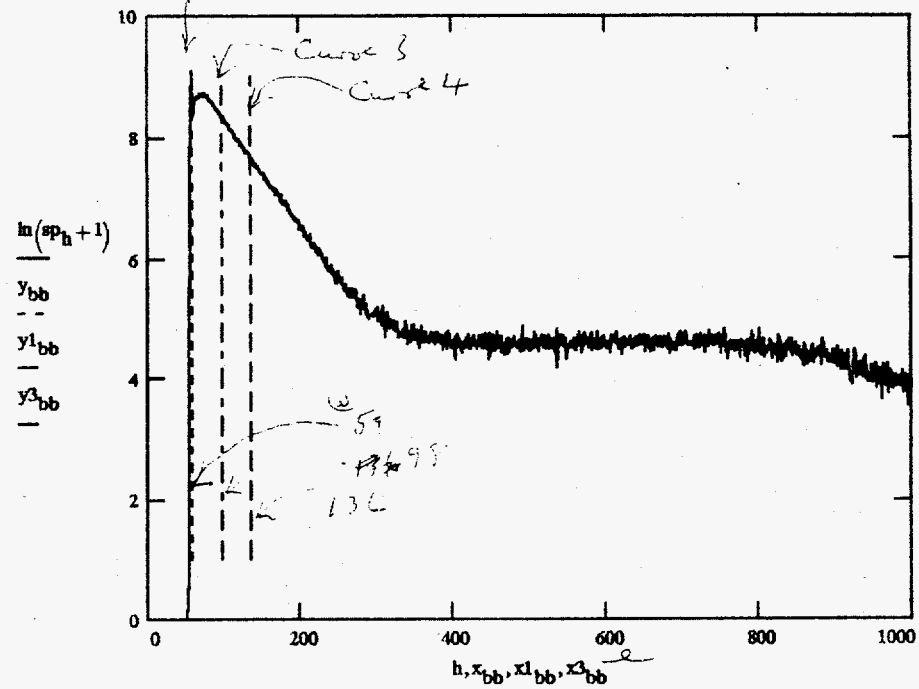

PREAMPL 19 NOV 96 This is an effort to consolidate the results of the dead time recovery study.
These results came from a Westinghouse 2 x 10" unkn press 1000 volts [SX-4470-554-7613]
1 usec time constant in PADM CHAN 2. Disc @ 0.317

$a := READPRN(krb01x) + READPRN(krb02x) + READPRN(krb03x) + READPRN(krb04x) + READPRN(krb05x) \ldots$
$+ READPRN(krb06x) + READPRN(krb07x) + READPRN(krb08x)$

$k := 0..2000 \quad s_k := READ(KRAA) \quad h := 0..900 \quad sp_h := s_{h+7} \quad i := 0..99 \quad L1 := \frac{1}{75} \cdot \sum_{q=25}^{99} a_q$

$L1 = 1.70575 \cdot 10^{3}$

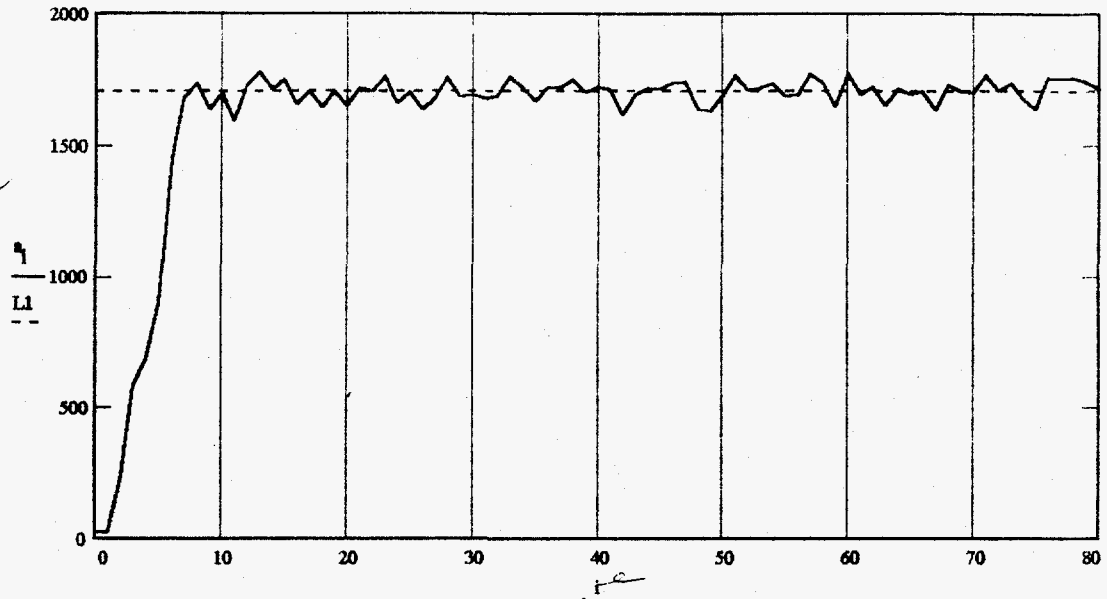

Fig 9a

Used in file sldfig9a.PRN

$M := 500 \quad x_0 := 117 \quad y_0 := 1$

$bb := 0..1 \quad x_1 := 117 \quad y_1 := M$

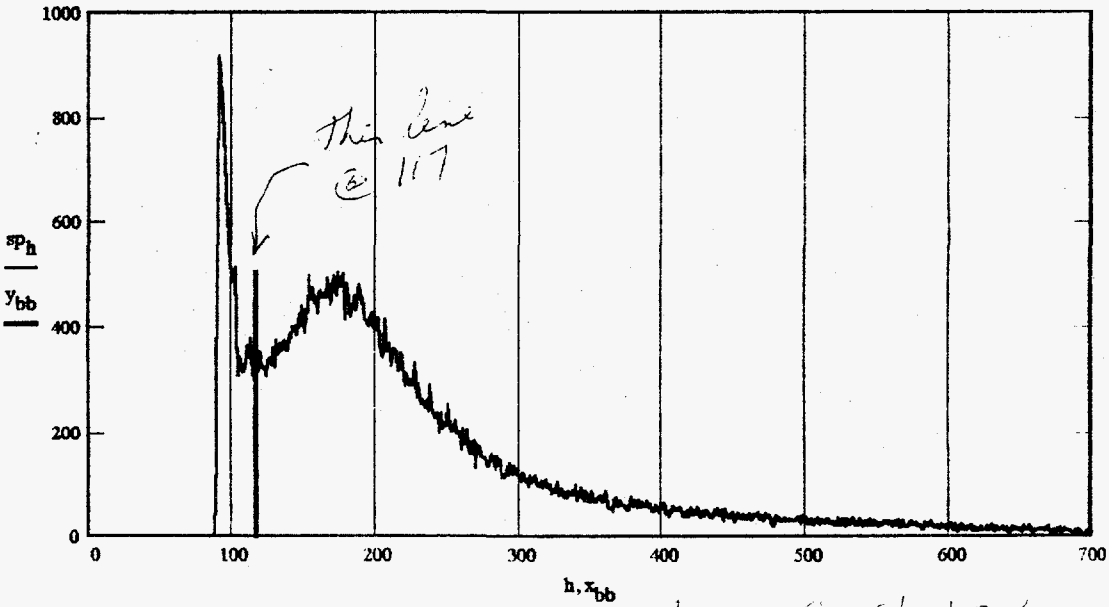

Fig 9b

In file sldfig9b.PRN

Pulse Height

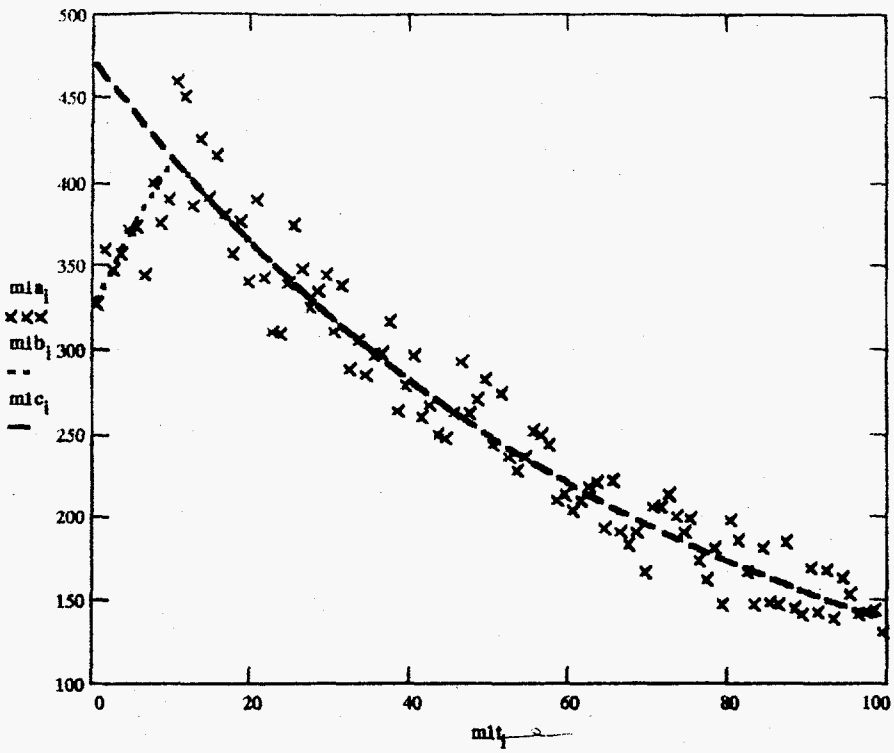
500
450
400
350
300
250
200
150
100
0
20
40
60
80
100
mia_i
mib_i
mic_i
mit_i

MSEC

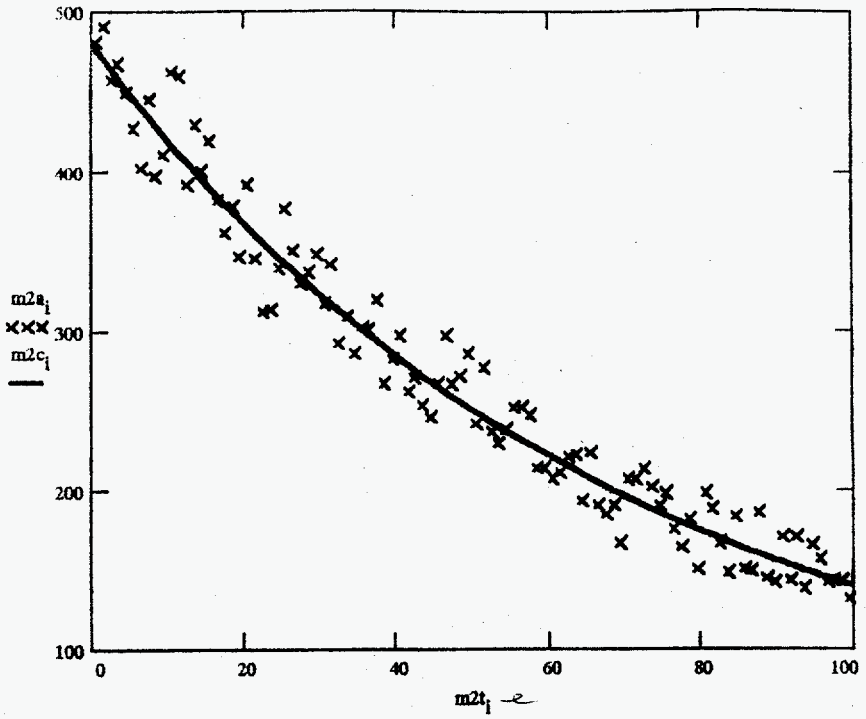
500
400
300
200
100
0
20
40
60
80
100
m2a_i
m2c_i
m2t_i
usec

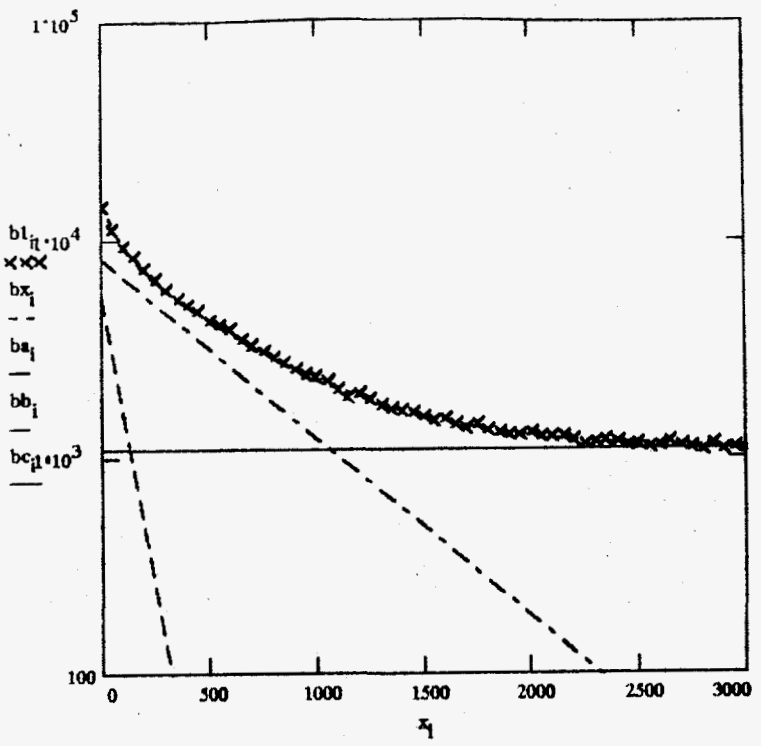

μSec

Fig. 6

Fig. 12

$\frac{bx_i - bl_i}{bx_i}$

0

0.0

0.

$w := 0..60$

$tmp_{w,0} := x_w$

$tmp_{w,1} := bl_w$

$tmp_{w,2} := bx_w$

$tmp_{w,3} := ba_w$

$tmp_{w,4} := bb_w$

$tmp_{w,5} := bc_w$

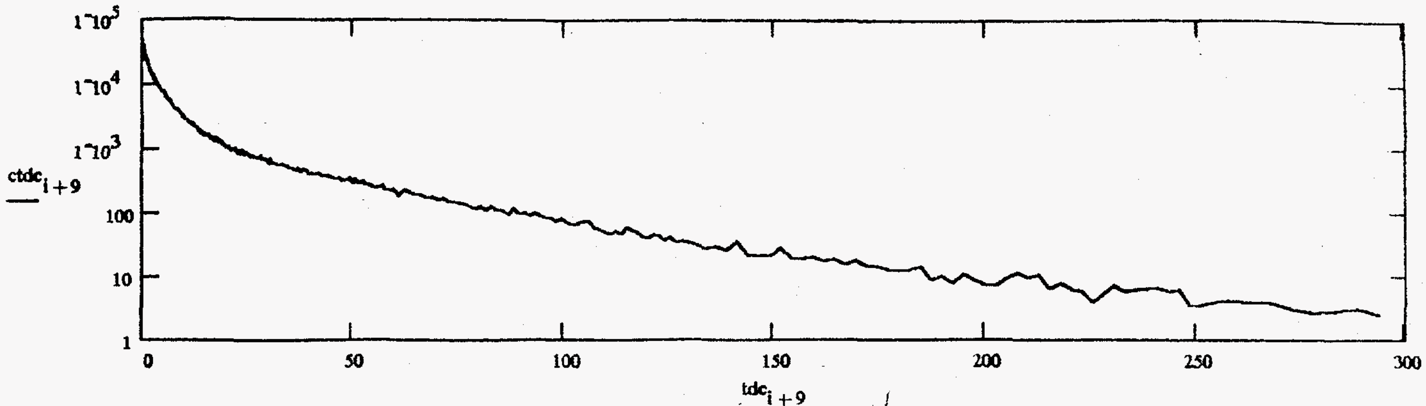

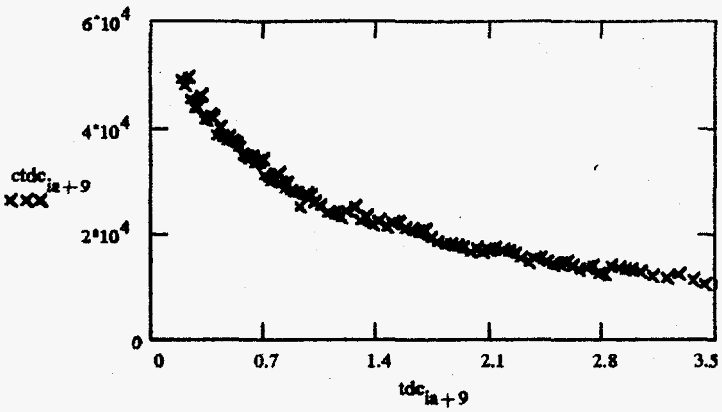

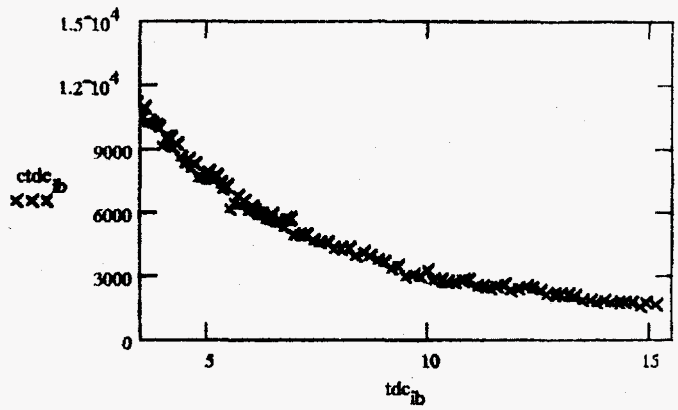

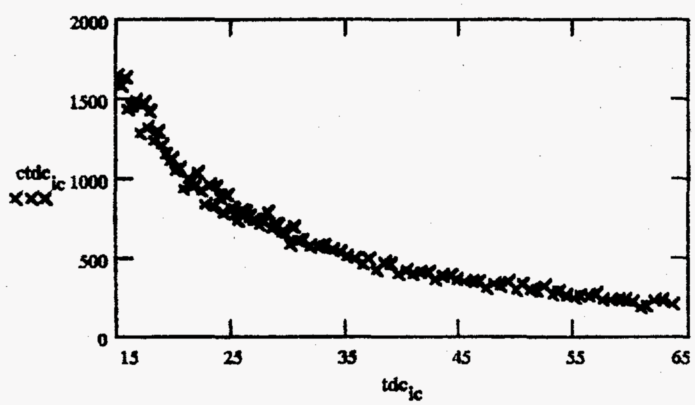

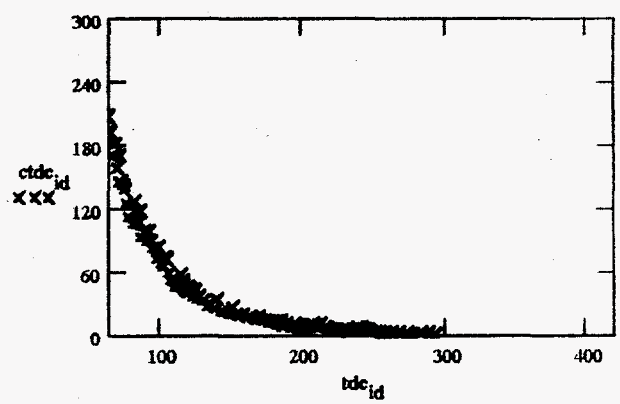

Data are in file SL1G14.PRN

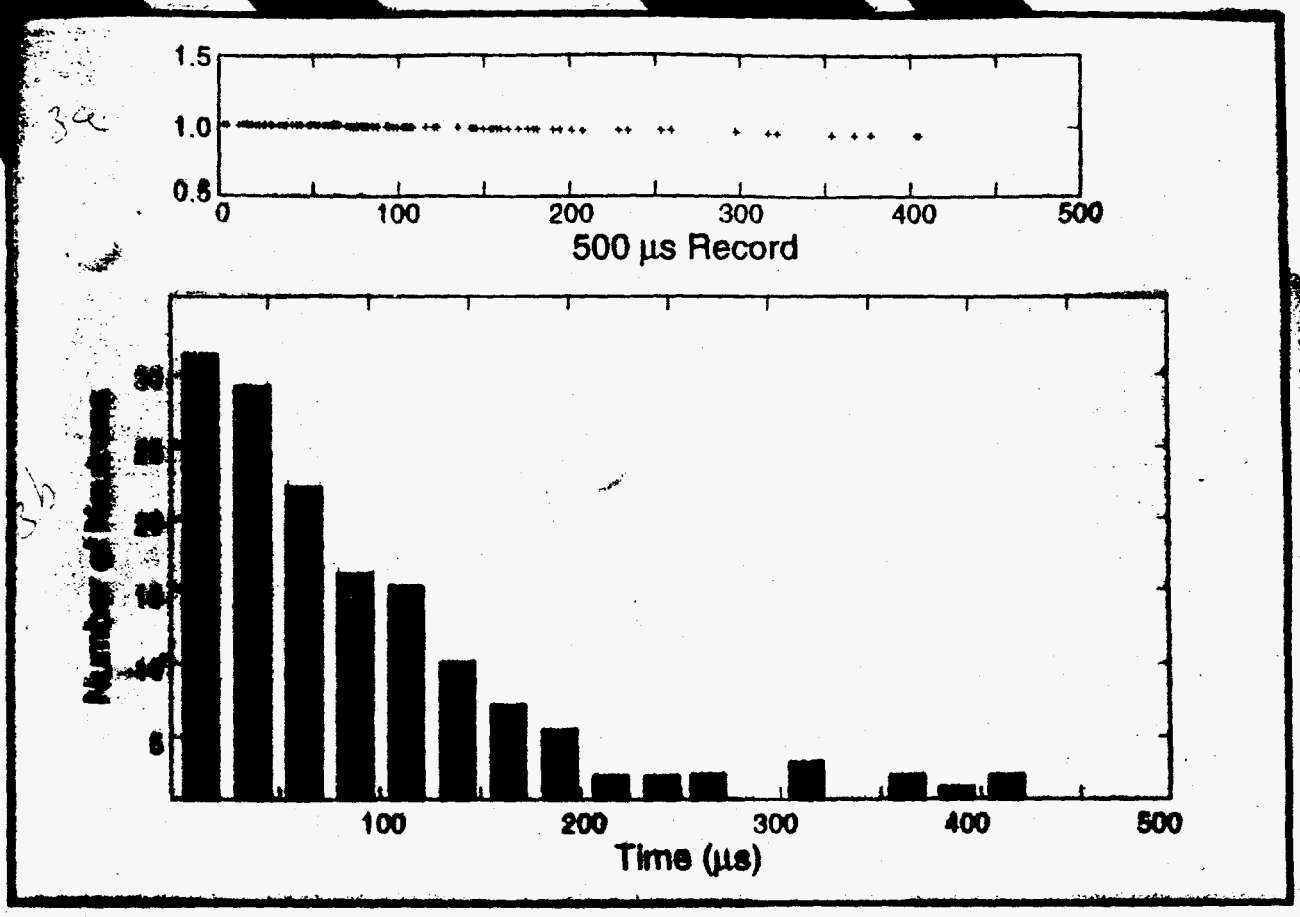
1.5
1.0
0.5
0
100
200
300
400
500
500 µs Record
100
200
300
400
500
Time (µs)